Research Square

Preprints are preliminary reports that have not undergone peer review.
They should not be considered conclusive, used to inform clinical practice,
or referenced by the media as validated information.

Fabrication and DC Characterization of BST-Gated AlGaN/GaN MOS-HEMT Structures in Two- and Three-Terminal Configurations

Abdullah

p22ee001@iitj.ac.in

Indian Institute of Technology Jodhpur, Rajasthan, India https://orcid.org/0000-0001-9487-2595

Research Article

Keywords: AlGaN/GaN HEMT, MOS-HEMT, BST gate dielectric, high-k dielectric, two-terminal device, three-terminal device, DC characterization

Posted Date: July 14th, 2026

DOI: https://doi.org/10.21203/rs.3.rs-10319963/v1

License: This work is licensed under a Creative Commons Attribution 4.0 International License.
Read Full License

Additional Declarations: The authors declare no competing interests.

Abstract

This study involves fabricating micro-scale two-terminal and three-terminal devices using the AlGaN/GaN HEMT platform, either with or without the high-k Barium strontium titanate oxide (BST) gate dielectric. Two-terminal devices are characterized by means of symmetric I-V (Current-Voltage) measurement ranging between − 1 V to 12 V to determine the effect of BST deposition on the leakage and conduction properties. On the other hand, three-terminal devices are characterized using transfer and output curves in order to extract critical parameters of the MOS HEMT device structure such as threshold voltage, on/off current ratio, transconductance. The fabricated devices yield a threshold voltage of about 0.028 V, on-current of order 10^{-8} A at V_{gs}= 0.7 V, and maximum transconductance of 4.0×10^{-6} S at V_{ds}= 20 V.

1. Introduction

Among many other wide-bandgap semiconducting materials, Gallium Nitride (GaN) is among the most significant wide-bandgap semiconductor materials used in modern power electronics, high-frequency communication circuits, radar, satellites communication equipment, and in the electric vehicles industry. In comparison with the traditional silicon-based semiconductors, GaN has an extensive bandgap, higher electric breakdown field, higher electron saturation speed, and enhanced thermal stability [1]. Due to such favorable physical properties, GaN devices can operate at increased voltages and frequencies as well as under high temperature without increased power losses and higher efficiency levels. Therefore, GaN has become increasingly popular due to its promising potential for replacing silicon technology in electronics [2].

The AlGaN/GaN HEMT is one of the widely investigated among many kinds of GaN-based electronic devices owing to its remarkable electrical characteristics. The AlGaN/GaN HEMT operation depends on the creation of the high-concentration of 2DEG at the interface between the AlGaN and GaN layers. The creation of the 2DEG layer occurs spontaneously as well as piezoelectrically, without any doping, and this causes the creation of high carrier density and high mobility of electrons [3, 4]. This feature gives high drain current ability, low on-resistance, high transconductance, and good high-frequency characteristics to the AlGaN/GaN HEMT.

Despite all the above-mentioned advantages, however, traditional Schottky gate AlGaN/GaN HEMTs are subject to various shortcomings that affect their overall efficiency and reliability. The direct contact of the metal gate electrode with the semiconductor layer is responsible for substantial gate leakage current, threshold voltage instability, surface state trapping, and current collapse. This becomes an even greater concern during high electric field regime operation. In addition, surface/interface traps are capable of trapping electrons, leading to threshold voltage fluctuations and degrading the quality of carrier transport [5].

To mitigate these constraints, MOS-HEMT structures have been developed based on the use of a dielectric material placed between the gate metal and the semiconductor layer. The introduction of the dielectric layer greatly reduces the gate leakage current because of the increase in the energy barrier between the gate material and the channel. Furthermore, the use of a dielectric layer leads to increased electrostatic control of the 2DEG channel, thereby providing enhanced threshold voltage stability, superior transconductance, greater on-off current ratio, and improved switching ability. Consequently, MOS-HEMT structures provide a promising solution for the design of GaN devices [6].

The performance of MOS-HEMT is influenced to a great extent by the characteristics of the dielectric material. The dielectric materials that possess the characteristic of high permittivity (high-k) are widely considered because of their high gate-channel coupling efficiency while exhibiting reduced levels of leakage current. Contrary to the usual dielectric materials, high-k dielectrics offer higher gate capacitance without demanding ultra-thin insulation layers, resulting in better channel modulation and lesser tunneling leakage mechanism [7]. Thus, many high-k dielectric materials like SiNx, Al_2O_3, HfO_2, ZrO_2, and $HfZrO_2$ have been explored as dielectric materials for GaN-based MOS-HEMT. However, exploration into other suitable dielectric materials is a promising topic of interest.

Among the new high-k dielectric materials that have gained prominence are those of $BaSrTiO_3$, also referred to as BST. This is due to BST having a very high dielectric constant, exceptional dielectric tunability, and desirable polarization properties. $BaSrTiO_3$ (BST) is one of the members of perovskite oxide material and has properties that surpass many of the traditional gate insulators [8]. The high dielectric constant found in $BaSrTiO_3$ promotes better electrostatic interaction between the gate electrode and the 2DEG channel. Moreover, BST acts as an insulator layer through which no electric charges can pass. As a result, there is less leakage and fewer interface issues. The addition of strontium to barium titanate leads to better stability and tunability of the dielectric, which makes BST ideal for advanced MOS-HEMT applications. Because of all these attributes, BST has the ability to enhance DC electrical properties such as threshold voltage, transconductance, and current modulation of AlGaN/GaN devices [9].

Despite the considerable advancements that have been made in the field of dielectric technology of GaN transistors, most of the previously published work has concentrated primarily on the use of common dielectrics like SiNx, Al_2O_3, HfO_2, $HfZrO_2$, and others based on oxide gate stacks. On the contrary, there is relatively less published information on BST used as a gate dielectric material in the AlGaN/GaN MOS-HEMT structure. Moreover, a large part of the existing literature is centered around the radio frequency (RF) performance, increase in breakdown voltage, ferroelectric behavior, passivation process, or device simulation optimization. Experiments exploring the effect of BST on the DC performance of the AlGaN/GaN structure are rare [10].

Hence, the present work will deal with the fabrication and DC characterization of the AlGaN/GaN MOS-HEMT structure employing BST as gate insulator in both two and three-terminal forms. The idea behind this research is to study the effect of the incorporation of BST as a high-k dielectric layer by analyzing

various parameters such as transfer characteristics, output characteristics, threshold voltage, transconductance, current modulation, and leakage. This comparison will be made between the devices before and after incorporation of BST in order to obtain a thorough insight into the use of BST as a gate insulator for AlGaN/GaN MOS-HEMTs [11].

Recently, GaN HEMT investigations focused heavily on dielectric engineering, ferroelectric gate stacks, optimized gate geometry, back-barrier structures, double channels, RF properties enhancement, threshold voltage manipulation, thermal reliability, and physics of two-dimensional electron gas. Among many gate insulators such as Al_2O_3, HfO_2, $Hf_{0.5}Zr_{0.5}O_2$ (HZO), SiNx, and ZrO_2, efforts were made in order to decrease gate leakage current, optimize gate controllability, increase the gain of the transistor, and enhance reliability. Similar progress was achieved by different scientists regarding passivated AlGaN/GaN and InAlGaN/GaN HEMTs using ferroelectric gates, substrates modification, and optimization of their channel. Nevertheless, there is still no sufficient number of researches in the field of BST-gated AlGaN/GaN MOS-HEMT devices. There is hardly any scientific literature devoted to BST gate dielectrics for AlGaN/GaN devices, including deposition and fabrication technology and DC electrical properties investigation [12].

Moreover, no such work comparing the electrical properties of two and three terminal BST-gated MOS-HEMTs in terms of their threshold voltages, drain currents, transconductances, gate leakage currents, and DC operation performances have been published until now. Moreover, there are no studies regarding the effect of BST layer formation on the AlGaN/GaN interface, transport phenomena, and characteristics of devices, before and after the formation of BST layer. This is the reason why fabrication and characterization of BST-gated AlGaN/GaN MOS-HEMT structures in two and three terminal configurations can be considered an important scientific topic today [13].

2. Device structure and fabrication

2.1 Epitaxial structure

The devices considered here have been realized using commercial AlGaN/GaN HEMT wafers available through MOCVD technology. The heteroepitaxy comprised of an AlGaN barrier layer on a GaN channel layer, which resulted in high carrier density 2DEG at the AlGaN/GaN interface owing to the polarization effects [1–5]. The heteroepitaxy wafer acted as the base substrate material for the fabrication of two-terminal devices as well as three-terminal MOS-HEMT devices using BST gates. AlGaN/GaN heteroepitaxy was chosen due to its good carrier transport characteristics and high electron mobility [14].

Two-terminal device design

Initially, two-terminal structures were made in order to analyze the electrical properties of the AlGaN/GaN structure before and after deposition of the BST film. Two-terminal structures involved the deposition of metal contacts patterned on the surface of the AlGaN/GaN wafer. Such structures were

mainly designed for determining the impact of BST dielectric on the I–V characteristics of the device and the nature of electrical conductivity [1–4].

Upon completing the deposition of the metal contacts and making the two-terminal structures, electrical tests were conducted to determine the initial electrical properties. Further, BST was deposited using RF sputtering in the area of the gate contact, and further electrical tests were carried out [5].

2.2 Three-terminal MOS-HEMT structure

Following the fabrication and characterization of the two-terminal structures, three-terminal BST-gated MOS-HEMT devices were fabricated. The MOS-HEMT architecture consisted of source, drain, and gate terminals formed on the AlGaN/GaN heterostructure. A BST dielectric layer was introduced between the gate metal and semiconductor surface to realize the MOS gate structure [13–14].

For gate formation, a Ni/Au gate stack was employed, consisting of 20 nm nickel and 90 nm gold. The source and drain ohmic contacts were fabricated using an Al/Cr/Au metal stack with thicknesses of 150 nm, 30 nm, and 250 nm, respectively. The incorporation of the BST dielectric layer provided electrical insulation between the gate metal and semiconductor surface, enabling improved gate control and reduced leakage current compared with conventional Schottky-gate HEMT structures.

The fabricated device has an approximate channel length of 100 μm and channel width of 25 μm, as estimated from the optical micrograph [15].

2.3 Fabrication process flow

Fabrication started with the surface preparation of the commercially available AlGaN/GaN HEMT wafer. In order to clean the wafer from any contamination such as particles and organics, the wafer was treated according to the RCA cleaning procedure that involves RCA-1 and RCA-2 cleaning processes. The next step in the fabrication process was rinse the sample in deionized (DI) water and dry it under nitrogen gas flow. Photoresist (PR) was spin coated on the wafer to form a uniform PR film [11]. A pre-bake step was followed where the excess solvent from the PR film was eliminated and better adhesion of the photoresist material was achieved. The wafer was then aligned with the appropriate photomask and UV lithography was employed to imprint a pattern on the photoresist film [13].

Subsequently, the wafer was dipped in a developing solution to strip off the exposed parts of the photoresist film. Metal stack for the source-drain contacts was deposited by thermal evaporation. Lift-off procedure was then applied where the wafer sample was immersed in acetone solution to eliminate the extra metals. Finally, the sample was rinsed with DI water and dried with nitrogen gas [14–15].

Subsequently, RTA was performed on the device at 870°C for 47 seconds in quartz tube furnace system in order to enhance the quality of metal/semiconductor contact and minimize the contact resistance. After completion of the RTA process, the electrical current-voltage (I–V) characteristics of the device were obtained [17–18].

The second step in fabricating this HEMT device is deposition of a thin film of $BaSrTiO_3$ (BST) in the gate region of the device. Subsequently, a second cycle of photolithography process was done in order to create the pattern of gate region. Here, the procedure involved spin coating of photoresist, followed by soft bake, alignment of mask of the gate, exposing it to UV radiation, developing the pattern of gate region, and obtaining the gate opening pattern [16]. Afterwards, thermal evaporation technique was utilized to deposit the gate metal (nickel and gold). Lift-off technique was again used here in acetone to strip off the unwanted metal and form gate electrode on the BST thin film. Finally, the sample was cleaned using DI water, dried using nitrogen gas, and characterized electrically using I-V measurement [19].

Electrical characterization through current-voltage (I-V) was done to analyze the electrical properties of the structures formed. The next process is the deposition of the BST thin films to integrate the dielectrics. In this study, the BST thin film was deposited via RF magnetron sputtering technique. This was accomplished by using the commercially available 2-inch BST target as the sputtering source. Again, electrical characterization was conducted to check the effect of the BST dielectric layer.

The final stage of the fabrication process involves photolithography to define the gate region. This is followed by the deposition of Ni (10 nm)/Au (50 nm) as the gate electrode. Al/Cr/Au (150 nm/30 nm/250 nm) stack was deposited as the source and drain electrodes to create the three-terminal MOS-HEMT devices as well as for two terminal device. Electrical characterization was then conducted to perform the DC analysis of the fabricated devices [20].

2.4 Optical microscopy

The optical microscopy technique was applied to check the quality of fabricated devices at various stages of the manufacturing process. Images were captured after the creation and annealing of the two-terminal devices to ensure successful definition of their structure and contacts [4]. Other images were also captured after deposition of BST on the gate area to analyze the quality and structure of the device. After the production of the three-terminal MOS-HEMT device and the second photolithography process, images were obtained to show that source, drain, and gate contacts have been successfully created [13]. The images indicated the absence of any defect, discontinuity, or metal bridging, which means that contacts were defined and electrically isolated before performing DC measurements.

Figure 2. (a) Optical image of the fabricated two-terminal AlGaN/GaN HEMT structure showing ohmic contacts on the device surface. (b) Optical image of the same device after BST deposition in the active region between the contacts. (c) Optical image of the three-terminal device obtained after second-stage lithography, showing the formation of the Ni/Au gate electrode on the structure in (b)

Optical micrograph of the fabricated three-terminal AlGaN/GaN HEMT device is shown in (Fig. 1 **(c))** [2]. The lateral metal pads on either side are the source and drain ohmic contacts, whereas the narrow metal strip in the middle is the gate contact obtained from the second lithography step [11]. The portion

between the source and drain contacts under the effect of the gate forms the channel area, which is responsible for current flow in the device [9, 16].

3. Electrical measurement methodology

Electrical characterization of the fabricated devices was done using a Keithley 2634B Dual-Channel SourceMeter Unit (SMU) by running in DC voltage sweep mode [21]. Electrical characterization of both two-terminal and three-terminal devices was done in two stages before and after integrating the BST dielectric into the device structures [22, 23].

In the case of two-terminal devices, current-voltage (I-V) characteristics were taken to determine how BST deposition influences electrical conduction properties of the AlGaN/GaN structure. Voltage sweeps with symmetric voltages were run from ± 1 V, ± 2 V, ± 4 V, ± 6 V, ± 8 V, ± 10 V and ± 12 V, and the current output from these voltages sweeps was obtained [24]. This was done both before and after deposition of BST to understand the effect of the BST dielectric layer on current output properties of the device.

For the three-terminal BST-gated MOS-HEMT devices, the output and transfer characteristics have been measured with the Keithley 2634B system. The output characteristics (I_{ds}–V_{ds}) were determined by sweeping the drain-to-source voltage for different gate voltages (V_{gs}): −4 V, − 3 V, − 2 V, − 1 V, 0 V, 1 V, 2 V, 3 V, and 4 V. To investigate the gate modulation effect, the transfer characteristics (I_{ds}–V_{gs}) were acquired by sweeping the gate voltage between − 4 V and 6 V, while the drain voltage was kept constant at V_{ds} = 0.01 V, 0.05 V, and 1 V, respectively [25, 26]. Such measurements were performed for DC characterization of the fabricated BST-gated AlGaN/GaN MOS-HEMTs. The measurement parameters were defined by a linear sweep of voltage with about 150 sweep points, 5 ms source-to-measure delay time, and 20 ms measurement time. All measurements were made at room temperature conditions [27].

4. Results and discussion

The two-terminal test structure was created on the surface of the AlGaN/GaN HEMT using photolithography technique on the gate access layer. This was accomplished using a multilayer metal stack of Al/Cr/Au layers, which were deposited and then followed by rapid thermal annealing (RTA) [28]. This process is used in most cases involving III-nitrides to create a low resistance ohmic contact in III-nitride structures. Without BST, the two-terminal test structure I–V characteristics show near linearity between voltages − 12 V and + 12 V, indicating the formation of an ohmic contact [29, 30]. After depositing a BST layer in the gate region, the device preserves its approximately linear I–V response over the same bias range, indicating that the conduction mechanism between the two terminals, however, the characteristics remain mainly ohmic in nature (Fig. 3**(a-g))**. Nevertheless, for a given voltage sweep, the current that flows are significantly lower, at least an order of magnitude smaller than what was recorded for the device without BST. This means that the resistance between the two terminals is significantly higher for the current device as a result of the addition of the high-k BST layer [31].

Output Characteristics

After the I-V measurement of the device using two terminals, a gate was formed on the BST-deposited AlGaN/GaN using a second level of photolithography followed by deposition of the Ni/Au (10/50 nm) metal layer through thermal evaporation [32]. The Ni/Au is responsible for creating the Schottky barrier on the BST/AlGaN surface where Ni plays an important role as the main barrier metal due to its high work function (~ 5.15 eV) that helps modulate the 2DEG channel [33, 34].

Characteristics of output (variation of drain current (I_{ds}) with V_{gs} with fixed value of V_{ds} = 20 V) for the fabricated three terminal HEMT structure are listed in Table-2 below [35]. When V_{gs} varies from − 4 V to + 6 V, there is a gradual increase of drain current from 4.715×10^{-4} A to 9.347×10^{-4} A, showing the effect of gate voltage control on drain current (Fig. 4**(a))**. This steady rise of I_{ds} with varying V_{gs} follows the normal transistor operation of an n-channel depletion mode HEMT, since a high value of gate voltage leads to the accumulation of a greater number of carriers in the 2DEG channel region, resulting in enhanced conductance of the channel region [36].

Transfer Characteristics

Transfer curves were obtained by sweeping V_{gs} from − 4 V to + 6 V at specific gate voltages (V_{ds}=-1 V, 0.01 V, and 0.05 V) producing a drain current (I_{ds}) equal to 1.301×10^{-5} A, 1.199×10^{-5} A, and 2.049×10^{-5} A, respectively. It is clear from the above findings that there is no significant increase in drain current even at relatively low gate biases due to the sub-milliampere condition **(**Fig. 4**(b))** [37, 38]. This is because of the fact that a high permittivity material (high-κ BST) is used as the gate material in order to alter the gate capacitance and interface charge distribution. Slight non-monotonic nature of the I_{ds} versus V_{gs} plot (decrease of the current from 1.301×10^{-5} A to 1.199×10^{-5} A with an increase up to 2.049×10^{-5} A at V_{ds}=0.05 V) can be attributed to interface traps formed at the BST-AlGaN interface or depletion of 2DEG at zero gate bias voltage [39].

In summary, the performance of the 3-terminal BST-gated AlGaN/GaN HEMT structure shows effective gate control of drain current in both output and transfer modes, thus proving the validity of the proposed device. In both cases, the values of Ids show similarity, thus demonstrating that a functional 2DEG is formed under the BST/AlGaN heterostructure [40].

The threshold voltage (V_{th}) was determined from the transfer characteristics as 0.0281 V at a drain current of 4.314×10^{-10} A. The on-state current (I_{ON}) was obtained as 5.7601×10^{-8} A at a gate-source voltage (V_{gs}) of 0.7 V, while the off-state current (I_{OFF}) was observed to be 3.475×10^{-9} A at V_{gs}=-4 V and V_{ds}=1 V. The maximum transconductance $(g_m)_{max}$ obtained for the fabricated structure was 4.0323×10^{-6} S, indicating that the gate modulates effectively the channel current [41]. The very small value of the threshold voltage means that the fabricated device almost approaches normally-on operation mode, which agrees with the fabrication process of the AlGaN/GaN HEMT channel. In addition, the small off-

state current indicates minimal leakage conduction, while the transconductance value verifies the existence of modulation of the two-dimensional electron gas (2DEG) channel by the gate terminal [42].

Table-1

Comparative I–V response of the two-terminal AlGaN/GaN device before and after BST deposition in the gate region

Sweep Voltage (V)	**Drain Current, $\varvec{I_D}$ without BST (A)**	**Drain Current, $\varvec{I_D}$ with BST**
-1 to 1 V	4.865×10^{-4} A	4.323×10^{-5} A
-2 to 2 V	0.0011 A	8.4929×10^{-5} A
-4 to 4 V	0.0028 A	1.755×10^{-4} A
-6 to 6 V	0.0049 A	2.6385×10^{-4} A
-8 to 8 V	0.00699 A	3.5273×10^{-4} A
-10 to 10 V	0.00865 A	4.324×10^{-4} A
-12 to 12 V	0.00985 A	5.1706×10^{-4} A

Table-2

Measured output characteristics of the BST-gated AlGaN/GaN HEMT for $V_{ds} = 0$--20V at various V_{gs} bias conditions.

Gate-to-Source Voltage, $\mathbf{V}_{\varvec{g}\varvec{s}}$(V)	Drain Current, $\mathbf{I}_{\varvec{d}\varvec{s}}$(A)
-4 V	4.715×10^{-4} A
-3 V	5.385×10^{-4} A
-2 V	6.002×10^{-4} A
-1 V	6.605×10^{-4} A
0 V	7.193×10^{-4} A
1 V	7.788×10^{-4} A
2 V	8.352×10^{-4} A
3 V	8.870×10^{-4} A
4 V	9.347×10^{-4} A

5. Conclusion

The development of micro-scale two-terminal and three-terminal AlGaN/GaN devices incorporating a 200 nm sputtered BST layer at the gate region has been accomplished through photolithography, thermal evaporation, CVD rapid thermal annealing, and sputtering techniques. The I-V characteristics from two-terminal measurements prior to and following BST deposition reveal that the current is reduced by an order of magnitude at low voltage sweeps, thereby proving the blocking property of the BST layer. From three-terminal MOS HEMT measurements, a threshold voltage close to zero (0.0281V) and an on/off ratio of ≈ 16 have been measured, as well as a maximum transconductance of 4.0 $\times$ 10^{-6} S when V_{ds}=20V.

Declarations

Conflict of Interest:

The authors declare that there are no conflicts of interest regarding the publication of this manuscript.

Funding

Financial assistance provided by the Defence Research and Development Organisation (DRDO), Government of India by Department of Electrical Engineering, Indian Institute of Technology Jodhpur through the project titled “Radiation hard Gallium Nitride transistor for IoT enabled dosimeter” with Project No. S/DRDO/MK/20210075 is gratefully acknowledged. The author was supported as Junior Research Fellow (JRF) from February 14, 2022 to July 20, 2022 and further as PhD fellow from July 22, 2022 to December 15, 2023 under the above-stated project.

Acknowledgement

The author gratefully acknowledges Prof. Mahesh Kumar, Department of Electronics Engineering, and Central Research Facilities of IIT Jodhpur for providing laboratory facilities and research infrastructure during the period in which part of this work was carried out.

References

1. Bai Z, Chai S, Zhao C, Wang L (2023) Design of High Baliga’s Figure-of-Merit P-GaN Gate AlGaN/GaN Heterostructure Field-Effect Transistors with P-AlGaN Field Plates. J Electron Mater 52:3892–3902. https://doi.org/10.1007/s11664-023-10378-x
2. Tadjer MJ, Anderson TJ, Hobart KD, Mastro MA, Hite JK, Caldwell JD, Picard YN, Kub FJ, Eddy CR Jr (2010) Electrical and Optical Characterization of AlGaN/GaN HEMTs with In Situ and Ex Situ Deposited SiNx Layers. J Electron Mater 39(11):2452–2458. https://doi.org/10.1007/s11664-010-1343-9
3. Hao L, Xu K, Guo H, Shao P, Ye J, Zhou Y, Liu B, Lu H, Zhang R, Zheng Y, Chen D (2025) Enhanced performance of normally-off AlGaN/GaN MOS-HEMTs taking advantage of extreme-k $BaTiO_3$ with prominent dielectric polarization. Appl Phys Lett 127(6):062103. https://doi.org/10.1063/5.0277628
4. Murugapandiyan P, Kalva SRK, Revathy A, Fletcher A (2024) Enhancement Mode AlGaN/GaN MISHEMT on Ultra-Wide Band Gap β-Ga_2O_3 Substrate for RF and Power Electronics. J Electron Mater 53:2973–2987. https://doi.org/10.1007/s11664-024-11005-z
5. Amen MT, Tran DP, Feroze A, Cheah E, Thierry B (2025) Exploring the Effects of Barrier Thickness and Channel Length on Performance of AlGaN/GaN HEMT Sensors Using Off-the-Shelf AlGaN/GaN Wafers. Appl Sci 15(23):12751. https://doi.org/10.3390/app152312751
6. Wang Q, Chen CX, Li W, Qin YB, Jiang LJ, Feng C, Wang Q, Xiao HL, Chen XF, Liu FQ, Wang XL, Xu XG, Wang ZG (2021) Fabrication and Characterization of AlGaN/GaN HEMTs with High Power Gain and Efficiency at 8 GHz. J Semicond 42(12):122802. https://doi.org/10.1088/1674-4926/42/12/122802
7. Hassan S (2025) Gallium Nitride Transistors for Power Switching Applications. PhD Thesis, James Watt School of Engineering, Electronics and Nanoscale Engineering, University of Glasgow, Glasgow, UK. Available at: https://theses.gla.ac.uk/85854/

8. Cheng Z, Pang CS, Wang P, Le ST, Wu Y, Shahrjerdi D, Radu I, Lemme MC, Peng LM, Duan X, Chen Z, Appenzeller J, Koester SJ, Pop E, Franklin AD, Richter CA (2022) How to Report and Benchmark Emerging Field-Effect Transistors. Nat Electron 5:416–423. https://doi.org/10.1038/s41928-022-00798-8
9. Kim HY, Kim J, Liu L, Lo CF, Ren F, Pearton SJ (2013) Electrical Characterization of ^{60}Co Gamma Radiation-Exposed InAlN/GaN High Electron Mobility Transistors. J Vacuum Sci Technol B 31(5):051210. https://doi.org/10.1116/1.4820129
10. Yu TH, Chen YL, Tsao YF, Hsu CT, Lu TF, Hsu HT (2025) Improved Ferroelectric Effects and Gate Controllability in $Hf_{0.5}Zr_{0.5}O_2$-Gated InAlGaN/GaN MIS-HEMTs Using ZrO_2 Seed Layers. J Electron Mater 54:1096–1103. https://doi.org/10.1007/s11664-024-11600-0
11. Li ND, Lin YC, Chen KW, Hsu HT, Tsao YF, Chang EY (2025) Novel Gate Fabrication Process Enhancing High-Frequency Operation in AlGaN/GaN HEMTs for Ka-Band Applications. IEEE J Electron Devices Soc 13:593–598. https://doi.org/10.1109/JEDS.2025.3584809
12. Venkatesan RS, Manickam R, Duraipandi B, Kottakkal Sugathan K (2024) Performance Analysis of AlN/GaN HEMTs on β-Ga_2O_3 Through Exploration of Varied Back Barriers: An Investigative Study for Advanced RF Power Applications. J Electron Mater 53:3887–3900. https://doi.org/10.1007/s11664-024-11100-1
13. Alim MA, Azad MOF, Rahman A, Ahmmed KT, Jarndal A (2025) Temperature-Dependent Characterization of 2-DEG for Single- and Double-Channel GaN on SiC HEMTs. J Electron Mater 54:6812–6827. https://doi.org/10.1007/s11664-025-12035-x
14. Deshpande G, Bhattacharya S, Ajayan J, Mounika B, Nirmal D (2024) A Review of GaN Channel-Based MOSHEMTs for Next-Generation Medium/Low-Voltage Rating and High-Speed RF Power Applications. J Electron Mater 53:xxxx–xxxx. https://doi.org/10.1007/s11664-024-11177-8
15. Hao L, Xu K, Guo H, Shao P, Ye J, Zhou Y, Liu B, Lu H, Zhang R, Zheng Y, Chen D (2025) Enhanced Performance of Normally-Off AlGaN/GaN MOS-HEMTs Taking Advantage of Extreme-k $BaTiO_3$ with Prominent Dielectric Polarization. Appl Phys Lett 127(6):062103. https://doi.org/10.1063/5.0277628
16. Wang Q, Chen CX, Li W, Qin YB, Jiang LJ, Feng C, Wang Q, Xiao HL, Chen XF, Liu FQ, Wang XL, Xu XG, Wang ZG (2021) Fabrication and Characterization of AlGaN/GaN HEMTs with High Power Gain and Efficiency at 8 GHz. J Semicond 42(12):122802. https://doi.org/10.1088/1674-4926/42/12/122802
17. Cheng Z, Pang CS, Wang P, Le ST, Wu Y, Shahrjerdi D, Radu I, Lemme MC, Peng LM, Duan X, Chen Z, Appenzeller J, Koester SJ, Pop E, Franklin AD, Richter CA (2022) How to Report and Benchmark Emerging Field-Effect Transistors. Nat Electron 5:416–423. https://doi.org/10.1038/s41928-022-00798-8
18. Zhang TJ, Li SZ, Zhang BS, Pan RK, Huang WH, Jiang J (2007) Optical Properties of RF Magnetron Sputtered $Ba_{0.65}Sr_{0.35}TiO_3$ Thin Films. Ceram Int 33(5):723–726. https://doi.org/10.1016/j.ceramint.2005.12.016
19. Sharma N, Nigam A, Lobanov D, Gupta A, Novikov A, Kumar M (2021) Mercury (II) Ion Detection Using AgNWs–MoS_2 Nanocomposite on GaN HEMT for IoT Enabled Smart Water Quality Analysis.

IEEE Internet Things J 8(18):14326–14334. https://doi.org/10.1109/JIOT.2021.3071382

20. Pandey V, Gupta A, Tripathy S, Kumar M (2024) IoT-Enabled hBN/AlGaN/GaN High Electron Mobility Transistor for Carbon Dioxide Monitoring. In: *Proceedings of the IEEE Sensors Conference*. IEEE. https://doi.org/10.1109/SENSORS60989.2024.10784655
21. Nigam A, Sharma N, Lobanov D, Novikov A, Kumar M (2020) Ultrasensitive Detection of Mercury Ions Under UV Illumination of MoS_2 Functionalized AlGaN/GaN Transistor. IEEE Trans Electron Devices 67(12):5693–5700. https://doi.org/10.1109/TED.2020.3030000
22. Wu YR, Singh M, Singh J (2006) Device Scaling Physics and Channel Velocities in AlGaN/GaN HFETs: Velocities and Effective Gate Length. IEEE Trans Electron Devices 53(4):588–593. https://doi.org/10.1109/TED.2006.870571
23. Watanabe T, Boubanga Tombet S, Tanimoto Y, Wang Y, Minamide H, Ito H, Fateev D, Popov V, Coquillat D, Knap W, Meziani Y, Otsuji T (2012) Ultrahigh Sensitive Plasmonic Terahertz Detector Based on an Asymmetric Dual-Grating Gate HEMT Structure. Solid State Electron 78:109–114. https://doi.org/10.1016/j.sse.2012.05.047
24. Sharma N, Nigam A, Dolmanan SB, Gupta A, Tripathy S, Kumar M (2022) 1T and 2H Heterophase MoS_2 for Enhanced Sensitivity of GaN Transistor-Based Mercury Ions Sensor. Nanotechnology 33(26):265501. https://doi.org/10.1088/1361-6528/ac5cff
25. Mishra UK, Parikh P, Wu YF (2002) AlGaN/GaN HEMTs—An Overview of Device Operation and Applications. *Proceedings of the IEEE* 90(6):1022–1031. https://doi.org/10.1109/JPROC.2002.1021567
26. Johnson W, Xu GH, Lin H, Zhang Y, Tarakji A, Kumar A, Yang A, Khan J, Gaska MA, Shur MS (2001) AlGaN/GaN Heterostructure Field-Effect Transistors Grown by Plasma-Assisted MBE. Solid State Electron 45(11):1979–1985
27. Zhang G, Feng S, Li J, Zhao Y, Guo C (2012) Determination of channel temperature for AlGaN/GaN HEMTs by high spectral resolution micro-Raman spectroscopy. J Semicond 33(4):044003. 10.1088/1674-4926/33/4/044003
28. Medinceanu PC, Antonescu AM, Enachescu M (2026) Is GaN the Enabler of High-Power-Density Converters? An Overview of the Technology, Devices, Circuits, and Applications. Electronics 15(3):510. https://doi.org/10.3390/electronics15030510
29. Yadav A, Flitsiyan E, Chernyak L, Hwang Y-H, Hsieh Y-L, Lei L, Ren F, Pearton SJ, Lubomirsky I (2015) Low and moderate dose gamma-irradiation and annealing impact on electronic and electrical properties of AlGaN/GaN high electron mobility transistors. Radiat Eff Defects Solids 170(5):377–385. 10.1080/10420150.2015.1010170
30. Chaudhary S, Mahapatra B, Pandey V, Patel C, Dubey M, Kumar M, Mukherjee S (2025) Ultrasensitive Detection of Hg^{2+} Ions with CVD Grown MoS_2-Functionalized MgZnO/CdZnO HEMT. IEEE Sens J 25(2):2048–2055. https://doi.org/10.1109/JSEN.2024.3504842
31. Watanabe T, Boubanga Tombet S, Tanimoto Y, Wang Y, Minamide H, Ito H, Fateev D, Popov V, Coquillat D, Knap W, Meziani Y, Otsuji T (2012) Ultrahigh Sensitive Plasmonic Terahertz Detector

Based on an Asymmetric Dual-Grating Gate HEMT Structure. Solid State Electron 78:109–114. https://doi.org/10.1016/j.sse.2012.05.047

32. Lorenz A, Derluyn J, John J (2011) Surface Treatment and Passivation of AlGaN/GaN HEMT. US Patent 8(062):931B2
33. Panda B, Dhar A, Nigam GD, Bhattacharya D, Ray SK (1998) Optical properties of RF sputtered strontium substituted barium titanate thin films. Thin Solid Films 332:46–49. https://doi.org/10.1016/S0040-6090(98)01012-8
34. Lossy R, Heymann P, Würfl J, Chaturvedi N, Müller S, Köhler K (2001) Power RF-Operation of AlGaN/GaN HEMTs Grown on Insulating Silicon Carbide Substrates. In: *Proceedings of the GaAs MANTECH Conference*, pp. 153–156
35. Eller BS, Yang J, Nemanich RJ (2013) Electronic Surface and Dielectric Interface States on GaN and AlGaN, J. Vac. Sci. Technol. A, vol. 31, no. 5, Art. no. 050807. https://doi.org/10.1116/1.4807904
36. Ambacher O, Smart J, Shealy JR, Weimann NG, Chu K, Murphy M, Schaff WJ, Eastman LF, Dimitrov R, Wittmer L, Stutzmann M, Rieger W, Hilsenbeck J (1999) Two-dimensional electron gases induced by spontaneous and piezoelectric polarization charges in N- and Ga-face AlGaN/GaN heterostructures. J Appl Phys 85:3222–3233. https://doi.org/10.1063/1.369664
37. Medjdoub F, Shinohara K, Thome F, Moon J-S, Chumbes E, Guidry MT, Mishra U, Zanoni E, Meneghini M, Meneghesso G, Pomeroy JW, Thingujam T, Kuball M (2024) Emerging GaN Technologies for Next-Generation Millimeter-Wave Applications, IEEE Microwave Magazine, vol. 25, no. 10, pp. 18–37, Oct. 10.1109/MMM.2024.3428188
38. Visvkarma AK, Sehra K, Chanchal R, Laishram A, Malik S, Sharma S, Kumar DS, Rawal S, Vinayak, Saxena M (May 2022) Impact of Gamma Radiations on Static, Pulsed I–V, and RF Performance Parameters of AlGaN/GaN HEMT. IEEE Trans Electron Devices 69(5):2299–2306. 10.1109/TED.2022.3161402
39. Martínez PJ, Maset E, Martín-Holgado P, Morilla Y, Gilabert D, Sanchis-Kilders E (Aug. 2019) Impact of Gamma Radiation on Dynamic RDSON Characteristics in AlGaN/GaN Power HEMTs. Materials 12 17, Art. 2760. 10.3390/ma12172760
40. Chang Y-C, Ho Y-L, Huang T-Y, Huang D-W, Wu C-H (2021) Investigation of Normally-Off p-GaN/AlGaN/GaN HEMTs Using a Self-Terminating Etching Technique with Multi-Finger Architecture Modulation for High Power Application, Micromachines, vol. 12, no. 4, Art. no. 432, Apr. 10.3390/mi12040432
41. Lei Z-F, Guo H-X, Zeng C, Chen H, Wang Y-S, Zhang Z-G (2015) Influence of heavy ion irradiation on DC and gate-lag performance of AlGaN/GaN HEMTs, Chin. Phys. B, vol. 24, no. 5, Art. no. 056103, May 10.1088/1674-1056/24/5/056103
42. Gopal V (Year) Fabrication of AlGaN/GaN HEMTs (ed) (2019) Rochester Institute of Technology (RIT), Rochester, NY, USA

Figures

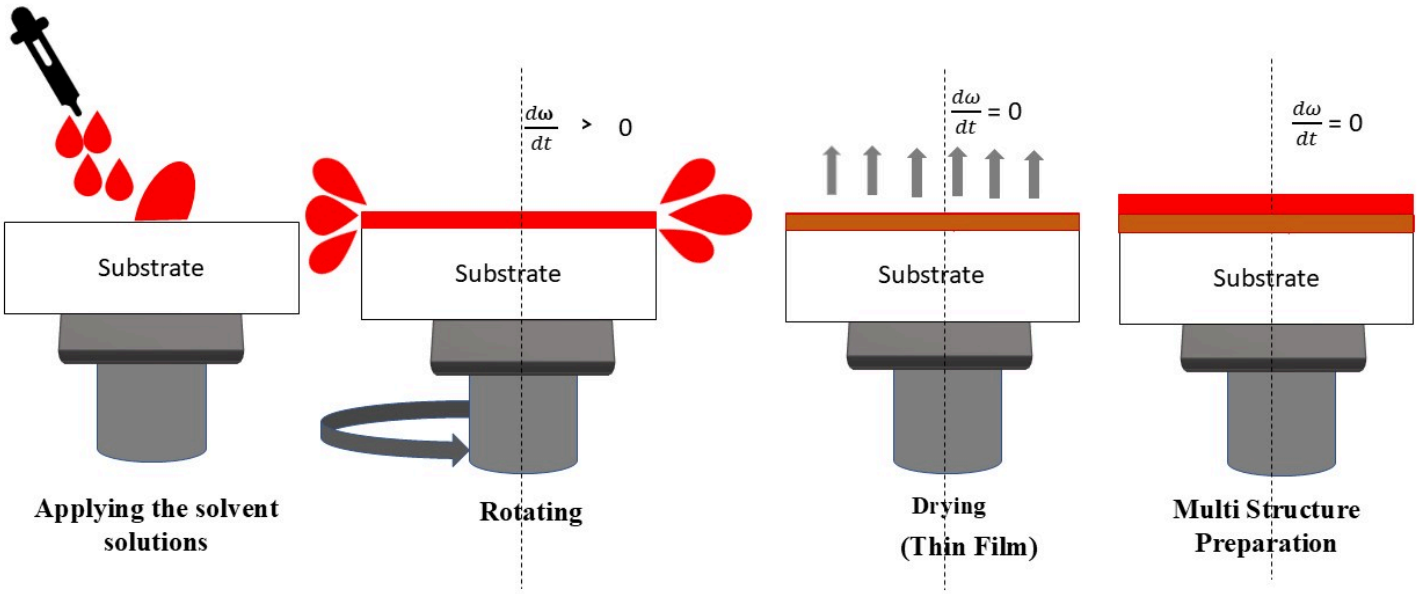


Figure 1

Fig. 1 Process flow of photoresist deposition by spin coating for photolithographic patterning. The photoresist is dispensed onto the substrate, uniformly distributed by high-speed rotation, and subsequently dried to form a homogeneous thin film suitable for UV exposure and pattern transfer.

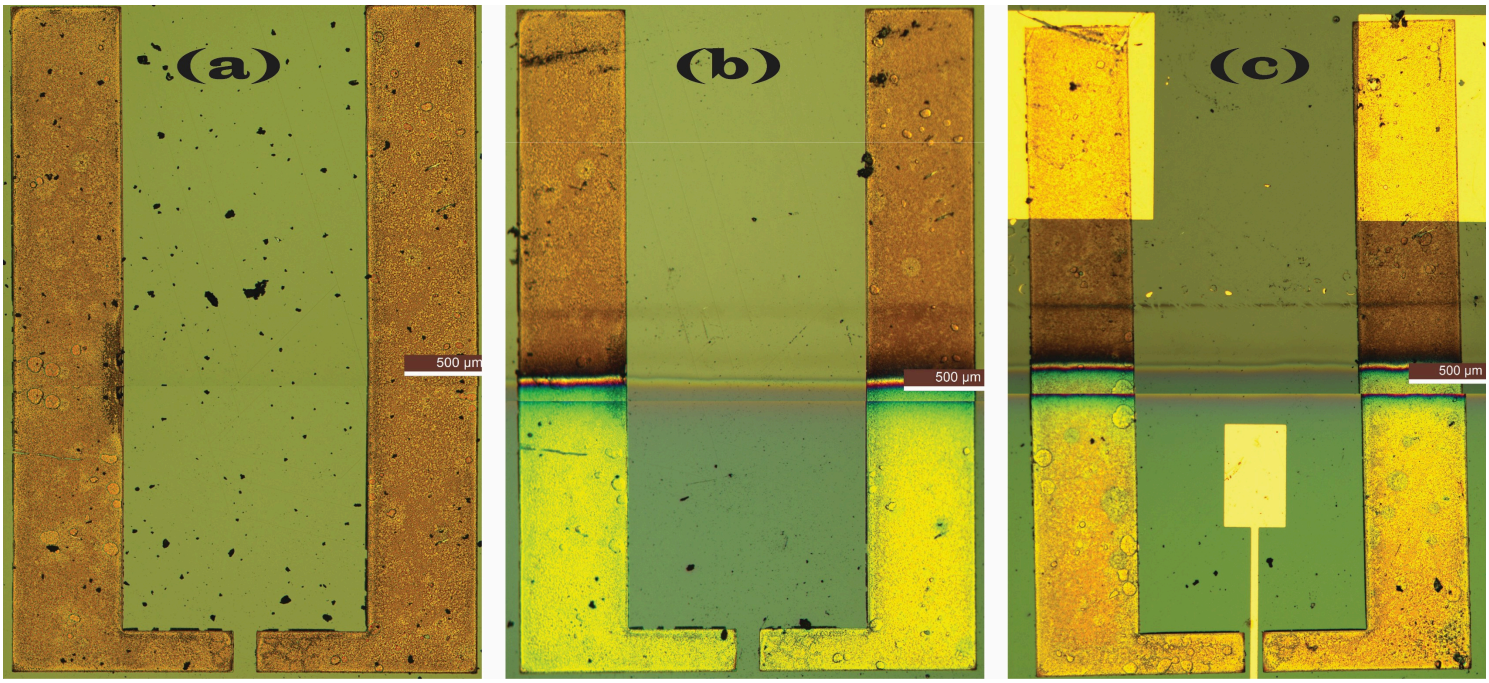


Figure 2

Fig. 2.(a) Optical image of the fabricated two-terminal AlGaN/GaN HEMT structure showing ohmic contacts on the device surface. (b) Optical image of the same device after BST deposition in the active region between the contacts. (c) Optical image of the three-terminal device obtained after second-stage lithography, showing the formation of the Ni/Au gate electrode on the structure in (b)

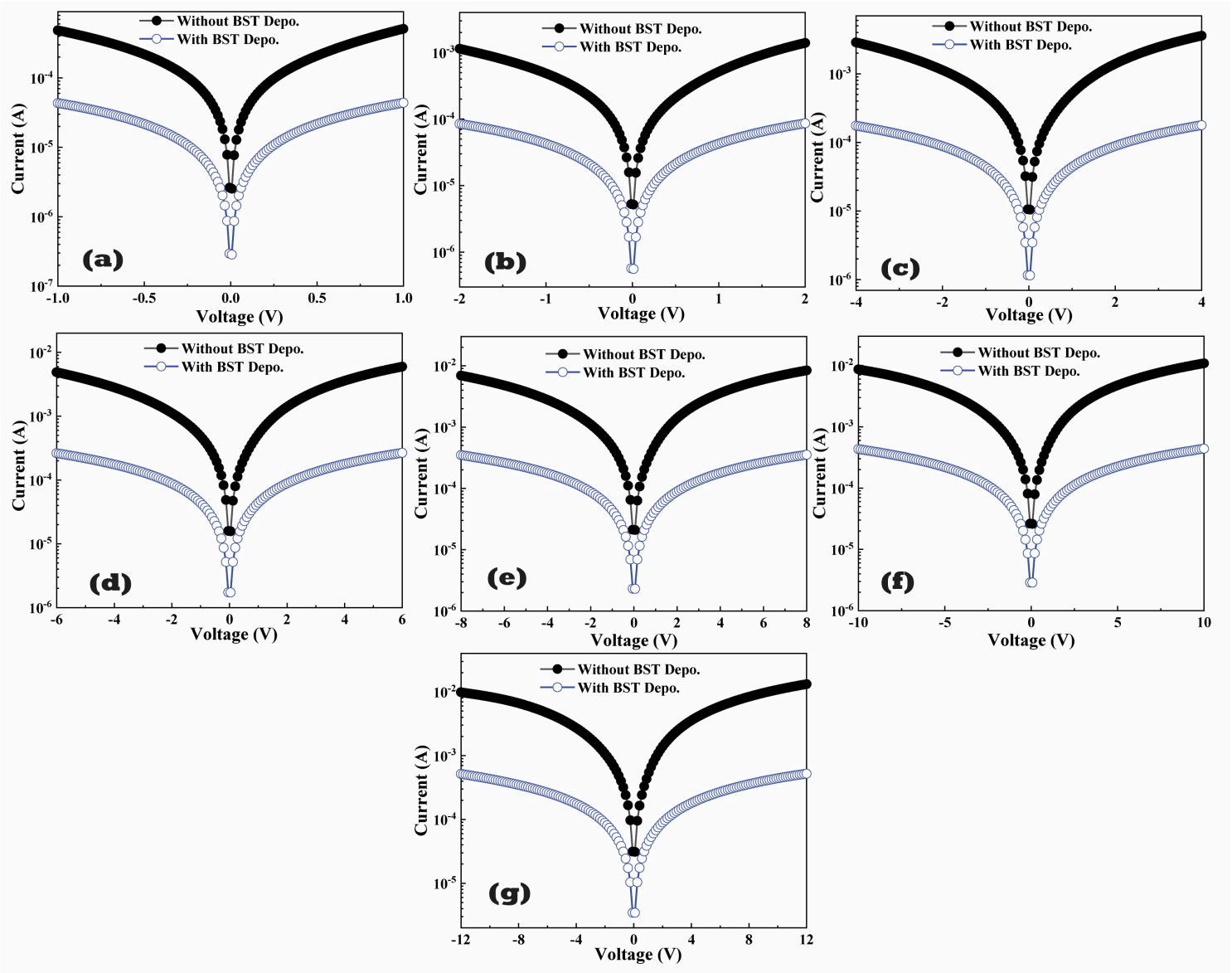


Figure 3

Fig. 3. I–V characteristics of the two-terminal AlGaN/GaN HEMT measured over different voltage sweep ranges: (a) −1 V to 1 V, (b) −2 V to 2 V, (c) −4 V to 4 V, (d) −6 V to 6 V, (e) −8 V to 8 V, (f) −10 V to 10 V, and (g) −12 V to 12 V.

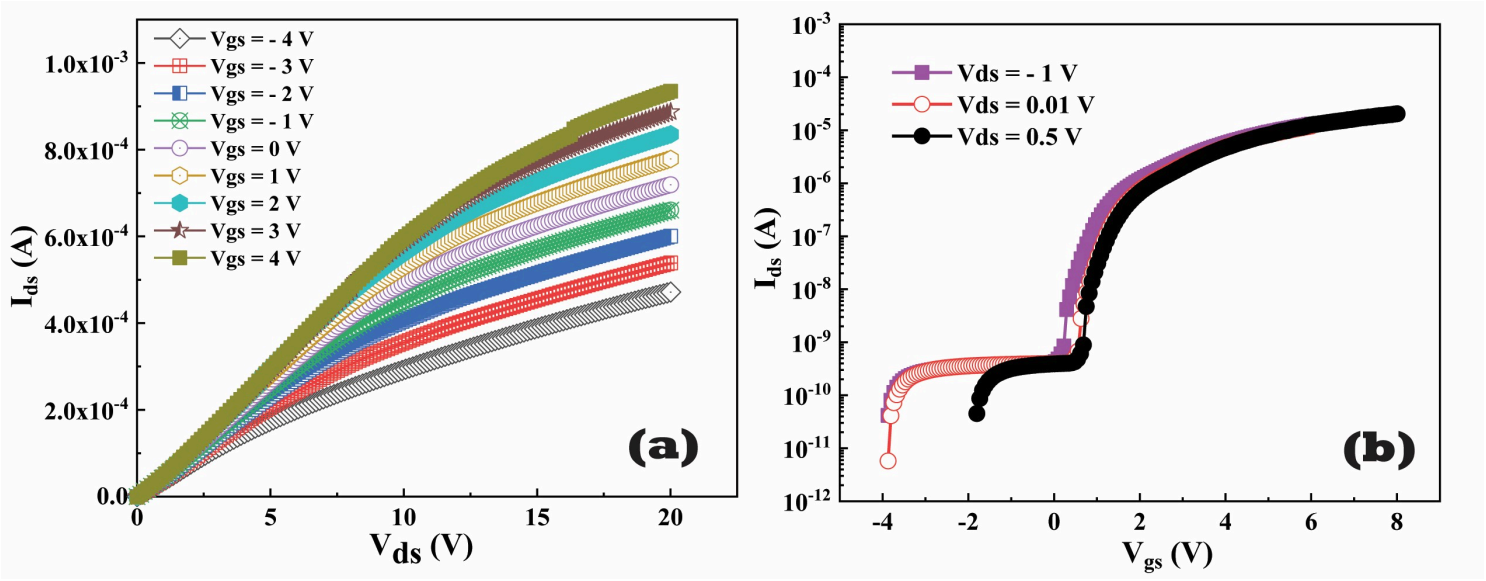


Figure 4

Fig. 4. (a) Output characteri**Fig. 4.** (a) Output characteristics $(I_{ds}–V_{ds})$ of the AlGaN/GaN HEMT at $V_{gs} = -4, -3, -2, -1, 0, 1, 2, 3,$ and 4 V; (b) transfer characteristics $(I_{ds}–V_{gs})$ measured at $V_{ds} = -1$ V, 0.01 V, and 0.5 V.stics $(I_{ds}–V_{ds})$ of the AlGaN/GaN HEMT at $V_{gs} = -4, -3, -2, -1, 0, 1, 2, 3,$ and 4 V; (b) transfer characteristics $(I_{ds}–V_{gs})$ measured at $V_{ds} = -1$ V, 0.01 V, and 0.5 V.